Compensation of Disturbances in Segmented Long Stator Linear Drives using Finite Element Models

R. Benavides, P. Mutschler
Dep. of Power Electronics and Control of Drives
Darmstadt University of Technology, Germany
rbenavid@srt.tu-darmstadt.de, pmu@srt.tu-darmstadt.de

Abstract- **Linear drives traveling on a carriageway with curves and closed paths are proposed for process integrated material handling. High precision and high throughput are required for this type of application. The long stator of the proposed permanent magnet synchronous machine is divided into many segments, each is fed by an inverter. When a vehicle enters a new segment, its EMF acts as a ramp-type disturbance for the current controller. Furthermore, asymmetries in the magneto motive force distribution are observed at the beginning and at the end of a segment. Also slot harmonics act as a considerable source of disturbance for the current control loop. To compensate these disturbances, the classical P-I current controllers should be supported by feed forward signals. In this paper, the feed forward signals are generated by a series of 2D Finite Element calculations. The geometrical data are taken from an experimental machine. As result of the FEM-calculations, look up tables where implemented in the control program and tested at the experimental setup. The experimental results show the effectivity of the feed forward.**

I. INTRODUCTION

Linear motors are known in many different designs and with a variety of different properties. Typically linear motors are used for straight-line movement of a single vehicle along a limited distance, e.g. in advanced machine tools. There is an increasing demand on flexible production plans, which can be adapted quickly to produce different products [1][2]. In order to cover the demands of flexibility we propose to extend the functional range of linear drives in several directions:

- On a carriageway several vehicles (work piece carriers) should be able to travel with a high degree of independency. Each vehicle has to be controlled very precisely when the vehicle operates within a processing station [3].
- The carriageway must allow for curves and for closed paths. In order to increase flexibility also switches shall be included in a future step.

In this paper, we discuss the compensation of disturbances caused by segmentation and slotting in long stator linear drives using feed forward signals obtained from FEM-calculations.

II. PROPERTIES OF THE MOTOR

The Long Stator Linear Synchronous Motor to be analyzed is made up by 8 double sided stator segments (Fig. 1). An outline of one segment is shown in Fig. 2. The windings of both sides are connected in parallel and fed by one inverter.

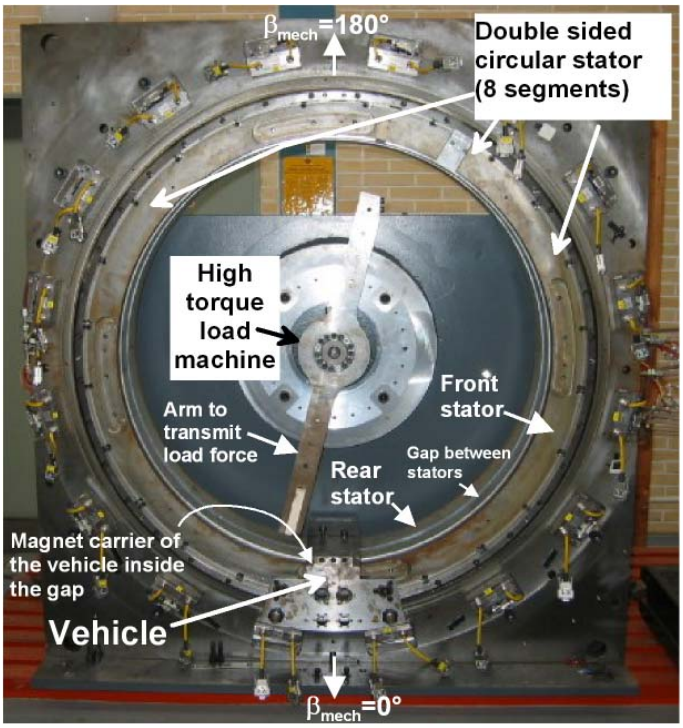

Fig. 1: Experimental machine.

Fig. 2 shows that each segment covers 45° of an annulus. A total of 8 segments form a complete annulus with an inner circumference of 3.12 meters. A top view of the unrolled stator and the mover is shown in Fig. 3. The winding arrangement forms a three-phase system with 6.5 pole pairs, the mover has 1.5 pole pairs.

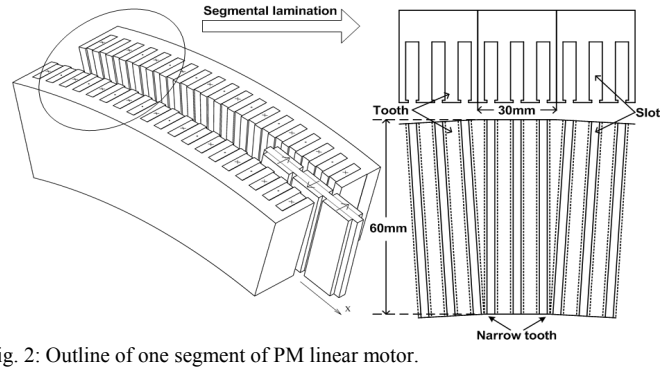

Fig. 2: Outline of one segment of PM linear motor.

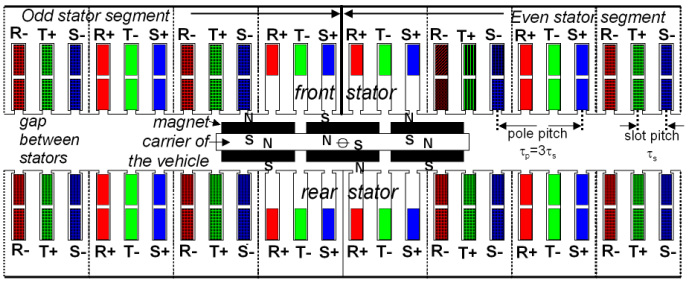

Fig. 3: Winding of the experimental machine.

A. Disturbances concerning current control.

When the mover enters a new segment with some speed, the induced voltage (EMF) in this segment rises from zero to its final value within 4 pole pitches. Likewise, the EMF in the previous sector decreases. Additionally, during this transition, the EMF in the three phases is unbalanced. If the speed is high, the change of the EMF is fast and may be approximated by a ramp. This ramp is a disturbance in the current control loop. A P-I current controller is unable to compensate a ramp type disturbance. Therefore, an EMF feed forward may be useful.

III. Calculation of the EMF by Finite Element Model

In some long-stator linear drives, the precise measurement of the no-load, speed-normalized EMF (1) is difficult, as the mover has to be moved by an external force and a speed or position sensor should be available, witch is not the case in speed sensor less control schemes.

$$\frac{\underline{e}_{abc}}{v} = \frac{\partial \underline{\Psi}_{abc}}{\partial x} \qquad (1)$$

Therefore, in this paper we use a Finite Element model to calculate (1). Generally, the fluxes are functions of currents (i_a, i_b, i_c) and position $x=(\tau p/\pi)\cdot\beta_m$, where τ_p is the pole pitch and β_m is the electrical angular position. This general case will be discussed in the last chapter, in the first step we deal with the no-load case ($i_a=i_b=i_c=0$). 2D Finite Element calculations are done at 648 mover positions, each shifted by 5°$_{electr}$ covering more than one segment. Fig. 4 shows the flux tubes when the mover is in the middle of the segment.

Due to the odd number of magnet poles at one side, the flux of one magnet will close through the large gap all around the annulus. But the field calculation can not be extended all over the annulus due to computation complexity and time. Therefore, the inactive segments are simplified to an equivalent reluctance. The field calculation delivers the fluxes Ψ_a, Ψ_b and Ψ_c as function of the position x. From these, feed forward quantities in mover aligned d-q-frame are calculated.

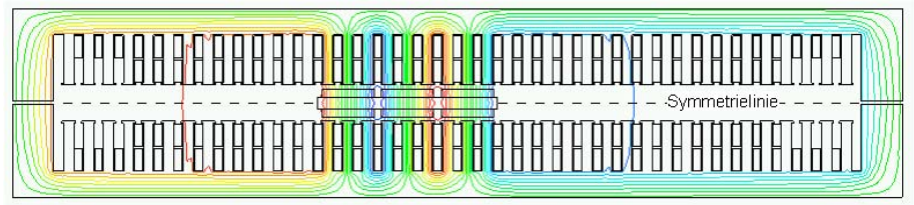

Fig. 4: Flux tubes of one segment without current exitation. The border conditions are as an equivalent reluctance on the complete annulus.

$$u_\alpha = R\cdot i_\alpha + \frac{d\Psi_\alpha}{di_\alpha}\cdot\frac{di_\alpha}{dt} + \frac{d\Psi_\alpha}{di_\beta}\cdot\frac{di_\beta}{dt} + e_\alpha \qquad (2)$$

$$u_\beta = R\cdot i_\beta + \frac{d\Psi_\beta}{di_\alpha}\cdot\frac{di_\alpha}{dt} + \frac{d\Psi_\beta}{di_\beta}\cdot\frac{di_\beta}{dt} + e_\beta \qquad (3)$$

$$e_\alpha = \frac{d\Psi_\alpha}{d\beta_m}\cdot\frac{d\beta_m}{dt} \qquad (4) \qquad e_\beta = \frac{d\Psi_\beta}{d\beta_m}\cdot\frac{d\beta_m}{dt} \qquad (5)$$

$$u_d = R\cdot i_d + \frac{d\Psi_d}{di_d}\cdot\frac{di_d}{dt} + \frac{d\Psi_d}{di_q}\cdot\frac{di_q}{dt} + e_d \qquad (6)$$

$$u_q = R\cdot i_q + \frac{d\Psi_q}{di_q}\cdot\frac{di_q}{dt} + \frac{d\Psi_q}{di_d}\cdot\frac{di_d}{dt} + e_q \qquad (7)$$

$$e_d = \left(-\Psi_q + \frac{d\Psi_d}{d\beta_m}\right)\cdot\frac{d\beta_m}{dt} \qquad (8) \qquad e_q = \left(\Psi_d + \frac{d\Psi_q}{d\beta_m}\right)\cdot\frac{d\beta_m}{dt} \qquad (9)$$

Fig. 5a shows the calculated e_α/ω and e_β/ω according (4) and (5). The calculated no-load speed normalized feed-forward quantities e_d/ω and e_q/ω according (8) and (9) are shown in Fig. 5b. The slot-harmonics, which are also disturbance quantities for the current control loop are clearly visible.

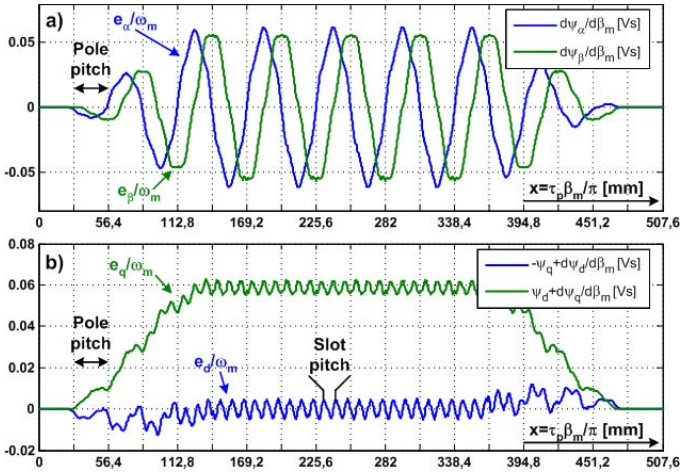

Fig. 5:Induced voltages at no load. FEM calculation.

IV. Experimental Results

At our experimental setup according to Fig. 1, a load machine in the center of the circle is used to stir the unloaded mover and an encoder is used for position measurement. With this setup, the induced voltage is experimentally attained and is shown in Fig. 6. When comparing Fig. 5 and 6, it must consider that the approximation for the boundary conditions discussed with fig. 4 can introduce an error. Additionally, the widths of the two air gaps at both sides of the mover are not precisely known and may be not identical.

Each third slot harmonic in the measured e_q (Fig.6b) has a higher amplitude. As shown in Fig.2, each third tooth is V-shaped in order to approximate the circle by a polygon. From this, each third tooth is very narrow at the inner circumference

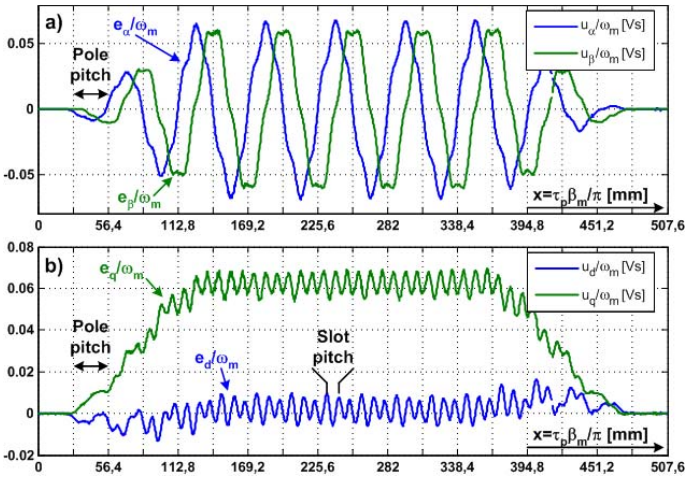

Fig. 6: Induced voltages at no load. Measurement.

and will be much higher saturated in the real machine than in the simulation, where all teeth have identical dimensions.

V. Feed Forward

Classical field oriented control is used. As shown by Fig. 7, the feed forward signals calculated as in Fig. 5b) where added to the outputs of the current controllers. The complete control loop is executed in a PC with a control cycle time of 100µs. In order to see the effectivity of the feed forward, the current references are set to zero in order to analyze the controller ability to reject perturbations.

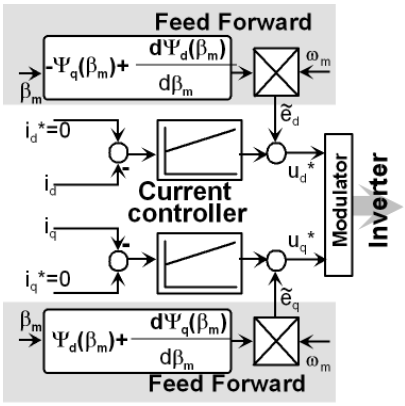

Fig. 7: Current controller with feed-forward.

Then, two experiments were carried out and compared in Fig. 8:
1) No feed forward but high bandwidth of the current control (fig. 8a).
2) Feed forward but very low bandwidth of current control (fig. 8b).

In spite of the high bandwidth, the current controller has difficulties to keep the q-axis current at its reference value when the mover enters the new stator segment and generates a ramp-type EMF disturbance, as can be seen at the left side of Fig. 8a). In the middle part of the sector, slot harmonics generate disturbances, which can no fully be compensated by the high gain current controller. In Fig. 8b) feed forward but very low bandwidth of current controller is used, such that the controller nearly does not counteract against the disturbances. The feed forward calculated by FEM reduces the current deviation when the mover enters the new stator segment as well as the deviations caused by slot harmonics.

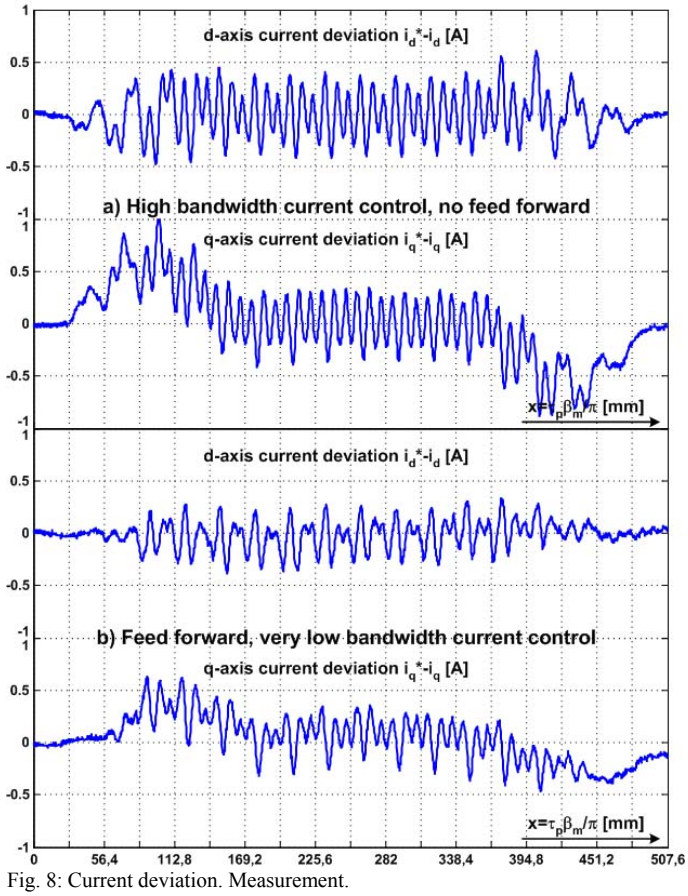

Fig. 8: Current deviation. Measurement.

VI. Improving the Dynamic Response to Setpoint Changes

Until now, only the EMF- terms in (8) and (9) were used. But the FEM-calculation delivers more results. Especially, the derivatives of the fluxes with respect to the currents – also known as differential inductances – i.e. (10) (11) and (12) may be used to calculate that amount of voltage from (6) and (7) which is necessary to change the currents within one sampling interval to the commanded set- point value.

$$L_{dd}^{diff}(i_d,i_q,x)=\frac{d\psi_d(i_d,i_q,x)}{di_d} \tag{10}$$

$$L_{dq}^{diff}(i_d,i_q,x)=\frac{d\psi_d(i_d,i_q,x)}{di_q} \tag{11}$$

$$L_{qq}^{diff}(i_d,i_q,x)=\frac{d\psi_q(i_d,i_q,x)}{di_q} \tag{12}$$

In general, fluxes and differential inductances are functions of two currents and the mover's position. To limit the number of field calculations to the really necessary ones, we can assume, that the d-axis current stays always close to its reference value[1]: $i_d=0$. This is justified by fig. 8b, where the peaks of i_d are about +-0.3A, which is 0.4% of the rated current (80A). With this consideration and neglecting the derivative of

[1] Field weakening is not discussed in this paper.

the current i_d, it is possible to rewrite (6) and (7) in a simplified voltage equations (13) and (14), where differential inductances L_{dq}^{diff} and L_{qq}^{diff}, fluxes Ψ_d and Ψ_q and their derivative are used.

$$\tilde{e}_d(i_q,x)=L_{dq}^{diff}(i_q,x)\cdot\frac{di_q}{dt}+e_d(i_q,x) \quad (13)$$

$$\tilde{e}_q(i_q,x)=R\cdot i_q+L_{qq}^{diff}(i_q,x)\cdot\frac{di_q}{dt}+e_q(i_q,x) \quad (14)$$

Then, the fluxes and differential inductances are functions of one current only and the position. For a given position, i_q is varied in 21 equidistant steps in the range of interest. For each of these i_q-values, the set of 3 stator currents i_a, i_b and i_c with i_d=0 is calculated. This set of currents are used as excitation for static 2D FEM field calculations. After this, the position is changed by 0.6 [mm] and the procedure is repeated there. A total of 601 different positions are used, which results in 21*601=12621 field calculations, covering a complete stator segment. From these calculations the flux linkages and the differential inductances are obtained. Each of these quantities is a 3-dimensional array. Each element of these arrays is then transformed to the d-q frame. The differential inductances L_{dq} and L_{qq} and fluxes Ψ_d and Ψ_q are shown in Fig. 9.

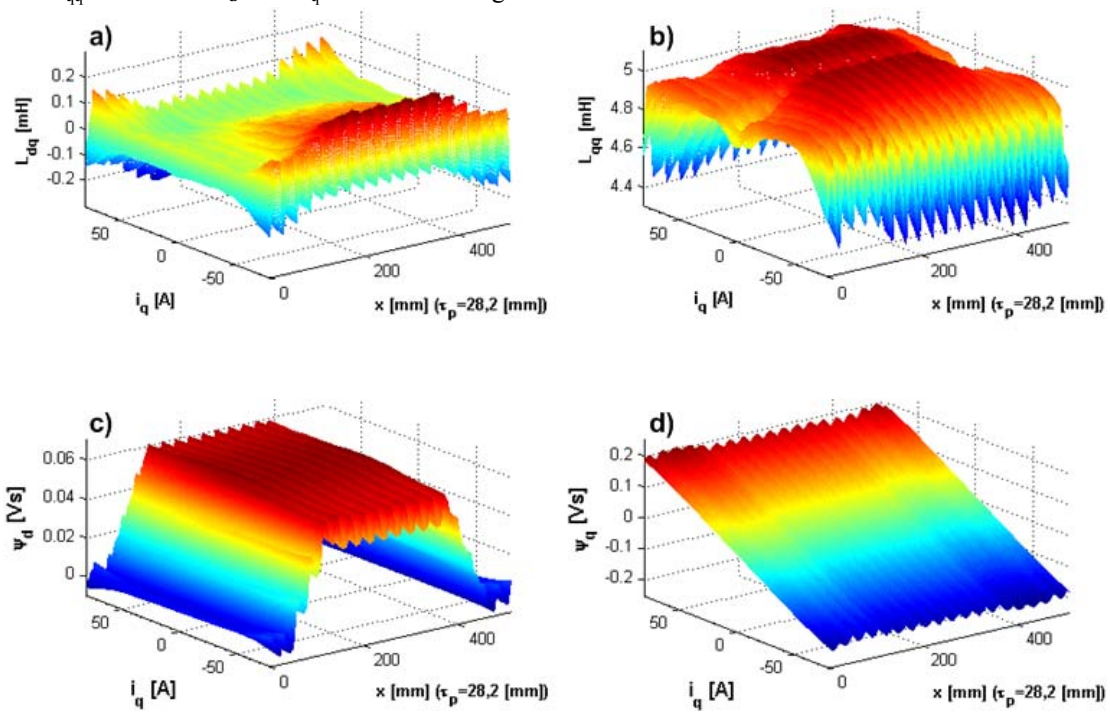

Fig. 9: Differential inductances and fluxes as function of the position in a complete segment and current i_q. FEM calculation.

To take a relation between the real inductance of the machine and the calculations, 50Hz sinus voltage was injected and the current was measured. The measurement give a phase resistance of 1.08Ω and an inductance of 6.3[mH]. In the construction of the machine, the magnets length is 80[mm] and the stator depth that cover the magnets is only 60[mm]. This produce a leakage inductance through the head of the

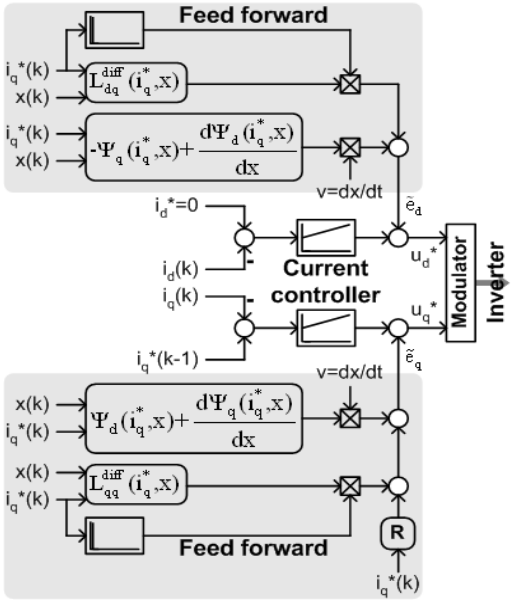

Fig. 10: Current controllers with feed forward.

windings. This explain the difference between the measurement and the calculation.

When the mover is outside of the segment, the flux Ψ_d is 0 (Fig. 9c) i.e. the induced voltage $e_q \approx 0$. The disturbances across the position are then due to the slot pitch.

These 3-dimensional look-up tables are used to calculate (13) and (14), and added to the output of the current controller. The resulting control loop is shown in fig. 10.

The feed forward model uses the current reference value i_q^* and the actual position x as input variables.

To avoid an overreaction of the PI controller, it's reference input was delayed by one sampling interval.

Figure 11 shows the current deviation for a change of 10[A] in the reference current i_q at the position x=169.2[mm]. For the high bandwidth controller without feed forward, the coupling component L_{dq} on the d axis introduce a disturbance that is not compensated (fig. 11a up). In this case, even a low bandwidth controller with feed forward present an important advantage.

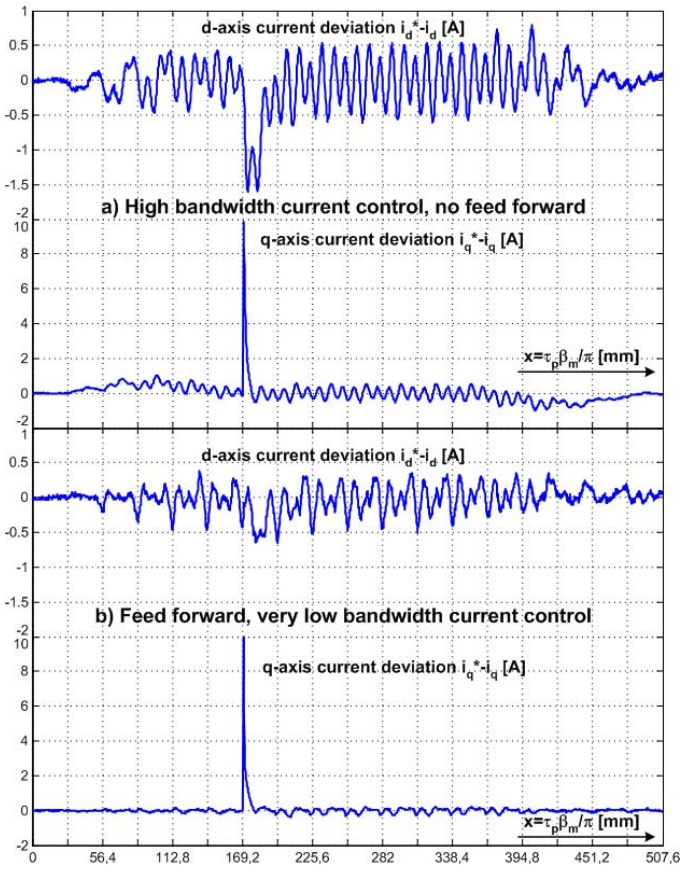

Fig. 11: Current deviation for a step in the current i_q of 10[A] at x=169.2[mm]. Reference current i_q* and position x are used as input to the feed forward control. Measurement.

The mutual inductance L_{dq} (fig. 9a) in linear machines can not be totally neglected, because it can produce complications when the machine is operated in field weakening mode.

In the q axes (fig. 11), the low bandwidth controller with feed forward presents a better slot-pitch oscillation rejection.

All the experiments were carried out by running the load machine of the setup (fig. 1) with a constant speed of 2.9[m/s] and using only one segment of the linear drive. Fig. 12 shows the voltages delivered by the model. In the d axis the slot-pitch

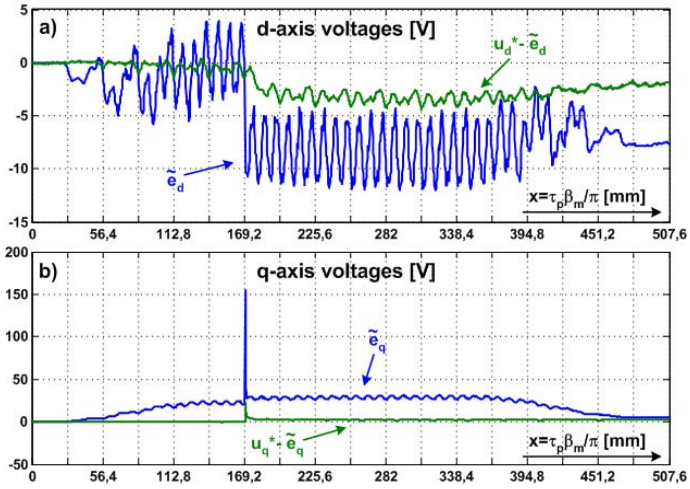

Fig. 12: model output voltages and controller output voltages. Measurement.

oscillation are well compensated for the model, reducing the stress on the current controller.

For the q axis, the model produces a spike for the current step. This reduces the reaction of the controller.

VII. Conclusion

Finite element models are well known tools for field calculations. To model a machine it is necessary to have a precise information of it. Geometry and sizes must be well known. After that, it must be decided whether a 2D static simulation is sufficient. For the model presented in this paper, a total of 12621 static 2D field calculation were done. It results in a high demand of computing time, in this case around one week using 3 PCs (3GHz). The mathematical error of the FEM model due to the grid was not discussed in this paper.

Feed forward control is a well known method to reduce the effect of disturbances. The machine presented in fig. 1 is a long stator permanent magnet linear motor with a high cogging force. This characteristic means a high effort for the current control. The feed forward model proposed, based on FEM calculations reduce the disturbances on the current loop and improve the dynamics on it.

Acknowledgment

The authors thank for the support of Deutsche Forschung Gemeinschaft, Project N°MU1109/12-1.

References

[1] N.A.Duffi, R.D.Lorenz, J.L.Sanders: "High performance LIM based material transfer." Proc. of the NSF Design and Manufacturing Systems Conf., Atlanta, GA, Jan 8-10, 1992, S.1027-1030

[2] G.H. Abdou, S.A.Sherif: "Theoretical and experimental Design of LIM in Automated Manufacturing Systems." IEEE Transactions on Industry Applications, Vol27, No2, March/April 1991

[3] R. Benavides, P. Mutschler : „Controlling a System of Linear Drives" Power Electronics Specialists Conference IEEE-PESC 2005 Recife, Brazil.